Photon-Induced Thermal Desorption of CO from Small Metal-Carbonyl Clusters

G. Lüttgens, N. Pontius, P. S. Bechthold, M. Neeb, and W. Eberhardt

Institut für Festkörperforschung, Forschungszentrum Jülich GmbH, 52425 Jülich, Germany

(Received 23 October 2001; published 30 January 2002)

Thermal CO desorption from photoexcited free metal-carbonyl clusters has been resolved in real time using two-color pump-probe photoelectron spectroscopy. Sequential energy dissipation steps between the initial photoexcitation and the final desorption event, e.g., electron relaxation and thermalization, have been resolved for $Au_2(CO)^-$ and $Pt_2(CO)_5^-$. The desorption rates for the two clusters differ considerably due to the different numbers of vibrational degrees of freedom. The unimolecular CO-desorption thresholds of $Au_2(CO)^-$ and $Pt_2(CO)_5^-$ have been approximated by means of a statistical Rice-Ramsperger-Kassel calculation using the experimentally derived desorption rate constants.

DOI: 10.1103/PhysRevLett.88.076102 PACS numbers: 68.43.Vx, 33.80.Eh, 36.40.–c, 42.65.Re

Thermal desorption of a molecule from an equilibrated surface takes place due to statistical energy fluctuations among all degrees of freedom. There is a certain probability that energy is accumulated in a specific chemisorptive bond that exceeds the desorption threshold of an adsorbed molecule. As thermal desorption is a statistical process, which is usually described in terms of stochastic time evolution of the energy content of the dissociative mode [1], the desorption rate depends first of all on the desorption threshold and the total number of degrees of freedom. In isolated particles, the energy cannot simply be released to the surrounding by diffusion or heat transport as in solids. Therefore in small metal-adsorbate clusters a finite probability exists to release the energy by thermal electron emission (thermionic emission) or thermal desorption of a ligand molecule after reaching thermal equilibrium. The energy redistributes either into a particular degree of freedom, i.e., a particular electronic state having one electron less, or a dissociative final state.

For photon-induced desorption processes, many dissipation steps are involved between the initial energy absorption and final ligand evaporation. Energy dissipation in photoexcited systems proceeds via electron relaxation and vibrational relaxation where the former process is usually faster than electron-vibrational coupling. Inelastic electron-electron scattering with time constants much less than 100 fs have been observed in optically excited bulk metals [2]. Similar relaxation times have also been observed for Pd and Au nanoparticles [3]. Even the smallest transition metal clusters of Pt, Pd, and Ni show electron relaxation times of about 100 fs [4,5]. Thermalization between the electronic and vibrational system is usually slower ranging to the ps regime.

Transition metal-carbonyl clusters such as $Pt_n(CO)_m^-$ are excellent candidates to study photon-induced thermal desorption processes. In these clusters decarbonylation thresholds are smaller than both the electron affinity (thermionic emission threshold) and the metal-metal dissociation energy [6,7]. Besides fluorescence, evaporation of a ligand molecule should thus be the only process by which energy can be released from carbonyl clusters.

Here, photon-induced thermal desorption from a cluster has been observed in real time for $Pt_2(CO)_5^-$ and $Au_2(CO)^-$ using pump-probe photodetachment spectroscopy. The low electron affinity of metal cluster anions allows one to monitor the chemically active metal core during desorption. In particular, the time-resolved photodetachment measurements of the mono-carbonyl-gold cluster exemplarily show the transition from a reacted cluster to a clean metal "surface" while CO desorption from the penta-carbonyl-platinum cluster shows the transition from a saturated to an unsaturated cluster. Our time-resolved data display directly the pathway and time scales of energy transfer from the hot electron system to the vibrational system. From the time-dependent photoelectron distribution on fs and ps time scales, it becomes evident that the primarily excited electronic state is fully thermalized before a CO ligand evaporates.

The experimental setup has been described in [8]. Unreacted metal clusters are produced in a laser vaporization source using a pulsed high pressure He-carrier gas. CO is injected via a second solenoid valve downstream of the cluster condensation zone. Anionic clusters are mass selected from the cluster beam with a time-of-flight mass spectrometer. When the desired carbonyl cluster anion enters the time-of-flight magnetic-bottle electron spectrometer [9], an electron is detached via pump-probe spectroscopy using two unfocused femtosecond pulses. The fundamental (1.5 eV) and second harmonic of a Ti:sapphire laser have been used as pump ($\sim$1 mJ, $\sim$80 fs, $\sim$4 mJ/cm^2) and probe ($\sim$0.3 mJ) pulses. The point of zero delay has been determined by polarization gating using the rear window of the spectrometer chamber (optical Kerr effect).

Figure 1 shows pump-probe photoelectron spectra of $Au_2(CO)^-$. The pump photon (1.5 eV) projects the occupied level density of ground state $Au_2(CO)^-$ onto the unoccupied one. This so-called joint density of states is monitored by the probe photon (3 eV) after a variable delay [5]. During this period, the dynamics within the photoexcited cluster is probed by the evolution of the photoelectron distribution. While a rapid decay for the

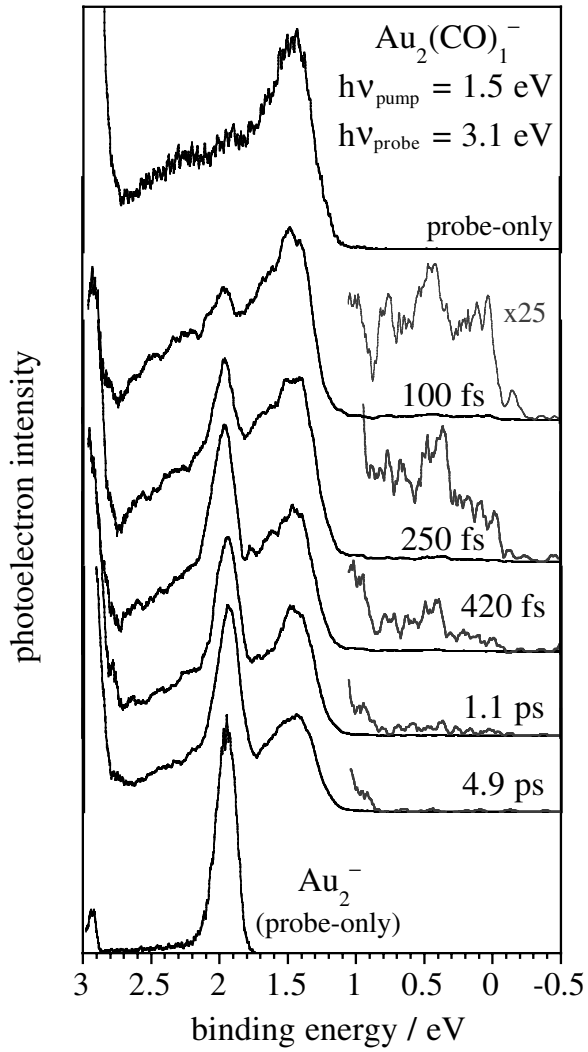

FIG. 1. Time-resolved pump-probe photoelectron spectra of $Au_2(CO)^-$. The probe-only (single-photon) photodetachment spectrum of $Au_2(CO)^-$ is shown at the top while the probe-only spectrum of Au_2^- is shown at the bottom.

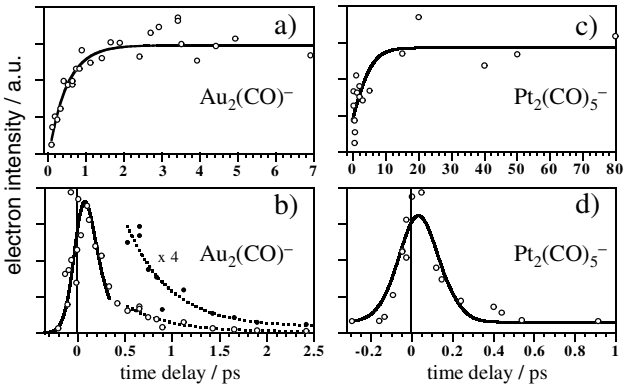

FIG. 2. Transient photoelectron intensities of $Au_2(CO)^-$ [(a) and (b)] and $Pt_2(CO)_5^-$ [(c) and (d)]. (a) Partial two-photon photoelectron intensity at 2 eV as a function of the delay. The transient peak intensity is directly related to the increase of the Au_2^- fragment. The full line shows an exponential fit from which the desorption time constant has been deduced. (b) Two-photon photoelectron intensity above HOMO (0–0.8 eV) as a function of the time delay. The fit (solid line) shows a convolution of the probe pulse and an exponentially decaying transient population (see text) from which the electron-vibration relaxation constant has been deduced. The lasting intensity drop above 400 fs indicates dissociation which has been fit by a single exponential (dashed line). (c) The intensity ratio of the vibrational components at 1.8 ($v = 0$) and 2.1 eV ($v = 1$) (see Fig. 3) as a function of the time delay. The transient shows the increase of the fragment $Pt_2(CO)_4^-$. From an exponential fit (solid line) the desorption time constant has been derived. (d) Two-photon photoelectron intensity above the HOMO (0–1.5 eV) of $Pt_2(CO)_5^-$ as a function of the time delay. The fit (solid line) shows a convolution of the probe pulse and an exponentially decaying transient population (see text) from which the electron-vibration relaxation constant has been deduced.

electron transients at low binding energies (<1 eV) is observed, a sharp peak evolves at 2 eV with increasing delay. This peak surmounts the underlying single-photon photoelectron spectrum (probe only) at delays larger than 200 fs. The emerging peak matches perfectly the photodetachment peak of unreacted Au_2^- (bottom of Fig. 1). Obviously, the photoexcited $Au_2(CO)^-$ cluster dissociates into ground state Au_2^- and CO. The position, width, and line shape of the Au_2^- peak does not change although the intensity continuously increases. Therefore we assume a statistical desorption of CO where the dissipated energy redistributes into a dissociative channel. An exponential fit to the transient intensity of the Au_2^- peak reveals a dissociation time constant $\tau_{\text{diss}} = (474 \pm 52)$ fs (Fig. 2a). Using the rate constant, $k(E^*) = 1/\tau_{\text{diss}}$, and applying a quantum Rice-Ramsperger-Kassel (RRK) formalism [10], $k(E^*) = \nu_{\text{vib}} \frac{j!(j-m+s-1)!}{(j-m)!(j+s-1)!}$, a dissociation energy $E_0 = 0.91$ eV is calculated where a vibrational frequency $\nu_{\text{vib}} = 1.16 \times 10^{13}$ Hz (48 meV) along the Au-C internuclear axis [11] and a maximum initial cluster temperature of $E_i = 300$ K were used [12]. In the RRK approach, it is assumed that the activated cluster with n atoms has $j = E^*/h\langle\nu_{\text{vib}}\rangle$ quanta of vibrational excitations, where $E^* = E_{h\nu} + E_i$ is the total energy of the cluster. s is equal to the number of vibrational degrees of freedom where $\langle\nu_{\text{vib}}\rangle = 53$ meV is the mean frequency of all vibrations of the cluster [11]. Dissociation along the Au-C coordinate requires $m = E_0/h\nu_{\text{vib}}$ quanta.

The quantum-RRK result is in good agreement with density functional calculations on bent $Au_2(CO)^-$ where a dissociation energy of 0.77 eV has been calculated [11] for the ground state potential. The bent geometry of the anion ($\sphericalangle$Au-C-O = 132.3°) is attributed to a Renner-Teller distortion of the degenerate lowest unoccupied molecular orbital (π) of neutral linear $Au_2(CO)$ [13]. The agreement between the RRK result and the quantum calculation supports our interpretation of a statistical loss of CO.

Besides the observed desorption dynamics, a preceding electronic relaxation of the "hot" electrons is evident from Fig. 1. This is obvious by the time-dependent photoemission intensity at binding energies below the electron affinity, i.e., at binding energies below 1 eV. In this energy region, the photoelectrons originate from photoexcited states. With increasing delay a shift from

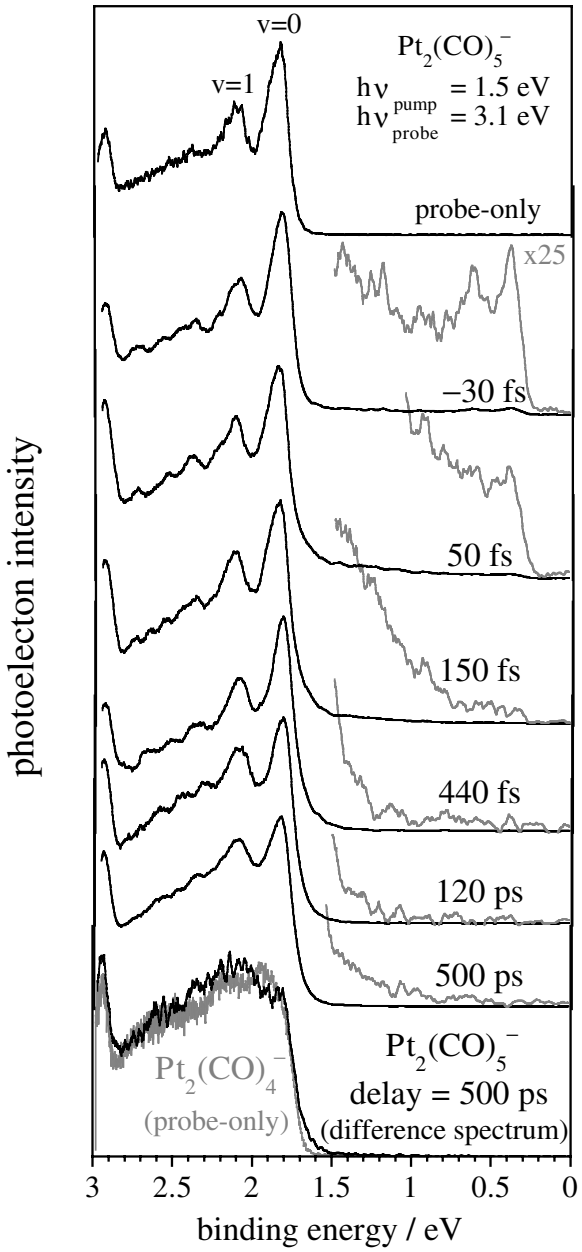

FIG. 3. Time-resolved pump-probe photoelectron spectra of $Pt_2(CO)_5^-$. The spectrum at the top shows the probe-only spectrum. At the bottom the probe-only spectrum of $Pt_2(CO)_4^-$ is shown together with the time-resolved spectrum of $Pt_2(CO)_5^-$ at 500 ps from which the contribution of direct photoemission (top spectrum) has been subtracted.

smaller to higher binding energies of the hot-electron intensity is observed. Such a dynamics is characteristic for inelastic electron scattering where the initially excited nonequilibrium population relaxes within the electronic system via scattering among various degenerate electronic states [2,5]. As long as the energy does not flow into the vibrational system, the relaxation leads to multiple-excited electron-hole pairs with secondary electrons excited at larger binding energies (inelastic scattering). The hot-electron intensity shifts towards the binding energy of the highest occupied molecular orbital (HOMO) as experimentally observed in the enlarged region of Fig. 1.

The electron-electron and electron-vibration relaxation times of the hot electrons can be extracted from the time-dependent hot-electron intensities. Applying a pure decay model, the probed photoelectron intensity as a function of the delay is $P(\Delta t) \propto \int_{-\infty}^{\infty} I(t - \Delta t)N(t)\,dt$, where $I(t - \Delta t)$ is the temporal intensity profile of the delayed probe pulse and $N(t)$ is the population as taken from a first order rate equation. From the fit of the integrated hot-electron intensity between 0 and 0.3 eV binding energy, an inelastic electron-electron scattering time constant of $\tau_{e\text{-}e} = (65 \pm 20)$ fs is deduced. The electron intensity in this binding energy range represents the electron population for which a pure decay by inelastic electron-electron scattering can be assumed [5]. This assumption is justified by the fact that electrons usually release half their excitation energy in a single scattering event leading to the removal of the electron from the integrated energy range [14]. Moreover, secondary electrons are not expected in that area due to energy conservation.

Not only the partial intensity but also the *total* two-photon electron intensity above HOMO decreases as is obvious by the intensity transient of Fig. 2b. This is interpreted by an energy transfer from the electronic to the vibrational system. A value of (126 ± 36) fs is revealed for the electron-vibration relaxation time constant $\tau_{e\text{-vib}}$ from a fit according to the above rate model. Note that the intensity of hot electrons still decreases continuously even after reaching thermal equilibrium. This lasting intensity drop is a result of CO evaporation by which the electron intensity of $Au_2(CO)^-$ continuously reduces. An exponential fit to the dropping intensity at a delay >300 fs reveals a thermal desorption time constant τ_{diss} of (455 ± 105) fs. This value agrees with the desorption time constant evaluated from the intensity transient of the Au_2^- peak.

Increasing the number of atoms, the time constant of thermal desorption should dramatically increase due to the larger number of vibrational degrees of freedom. Figure 3 shows time-resolved photodetachment spectra of $Pt_2(CO)_5^-$. The probe-only spectrum at the top reveals an adiabatic electron affinity of 1.8 eV. The first two peaks belong to a progression of the CO stretch vibration. The vibrational energy of ~263 meV hardly differs from that of free CO (269 meV). The vibrational splitting indicates an electronic saturation effect upon which the electronic configuration of Pt changes from $d^9s^1 \rightarrow d^{10}$ [15]. The extra electron of the anion is located in a π^*-derived CO orbital making the appearance of the CO stretch vibration on the adiabatic peak plausible.

The two-photon photoemission intensity at binding energies above the electron affinity, i.e., >1.8 eV, is strongly superimposed by direct photoemission of nonexcited $Pt_2(CO)_5^-$ (compare with probe-only spectrum at the top of Fig. 3). With an increasing delay a continuous change of the spectrum is recognized by a relative intensity increase above 2 eV and a reduction of the vibrational fine

structure indicating a fragmentation of $Pt_2(CO)_5^{-*}$ into $Pt_2(CO)_4^-$ and CO. Usually vibrational splitting does not occur on the leading photoemission feature of unsaturated platinum-carbonyl clusters, such as $Pt_2(CO)_4^-$ [15]. This is demonstrated in Fig. 3 (bottom panel) where the normal photodetachment spectrum of $Pt_2(CO)_4^-$ is displayed. Only a smooth edge is seen at the position of the leading edge, but no vibrational fine structure. In the same plot the time-resolved photoelectron spectrum of $Pt_2(CO)_5^{-*}$ at 500 ps is shown from which the probe-only spectrum of nonexcited $Pt_2(CO)_5^-$ has been subtracted. The nearly perfect agreement between the two spectra supports the interpretation of photodissociation into $Pt_2(CO)_4^- + CO$.

Fitting an exponential curve to the decreasing intensity ratio of the vibrational peaks at $v = 0$ and $v = 1$, which is proportional to the increasing amount of $Pt_2(CO)_4^-$, a dissociation time constant τ_{diss} of (3 ± 2) ps is deduced (Fig. 2c). Using a Pt-C vibrational energy of 60 meV [6] and a maximum initial cluster temperature of 300 K, a quantum RRK analysis gives a desorption threshold E_0 of 0.60 eV (58 kJ/mol). This energy is comparable to the calculated Pt-CO dissociation energy of linear Pt_2CO (75 kJ/mol) [16] and half the terminal CO-dissociation energy of saturated $Pt_3(CO)_5^-$ (109 kJ/mol) [6]. We assume the loss of a terminal CO since the dissociation energy of bridged CO is distinctly larger, e.g., 210 kJ/mol (2.2 eV) for bridged Pt_2CO [6]. The calorimetric desorption heat of CO from a Pt(111) surface amounts to -118 kJ/mol [17] at a saturation coverage of $\sim$0.5 monolayer.

The desorption rate of $Pt_2(CO)_5^-$ is smaller than that of $Au_2(CO)^-$ by a factor of 6. This is due to the number of vibrational degrees of freedom which is larger for the pentacarbonyl ($s = 30$) than for the monocarbonyl ($s = 6$).

The intensity at binding energies smaller than 1.8 eV reveals an electron relaxation which precedes the thermal desorption of CO. This two-photon emission intensity, which is not observed in the probe-only spectrum (Fig. 3, top), belongs to detachment of hot electrons above HOMO. Near zero delay, the intensity above HOMO looks very similar to the single-photon photodetachment spectrum. With increasing delay, the hot electron intensity redistributes from lower to higher binding energies and finally decreases. As for $Au_2(CO)^-$, this evolution of the hot-electron distribution can be explained by inelastic electron scattering and thermalization due to electron-vibrational coupling. Fitting the transient intensity of hot electrons above the HOMO with the above rate model, a time constant $\tau_{e\text{-vib}}$ of (36 ± 12) fs is deduced (Fig. 2d). The thermalization between the electronic and the vibrational systems, which proceeds about 100 times faster than the desorption of CO, is completely independent from the desorption process itself.

In summary, thermal desorption of CO from small transition-metal clusters has been measured in real time. Sequential energy-dissipation processes such as inelastic electron scattering, electron-vibration relaxation, as well as thermal desorption have been resolved in the time-resolved photoelectron spectra. While CO desorbs from $Au_2(CO)^-$ with a time constant of $\sim$500 fs, the desorption constant of $Pt_2(CO)_5^-$ amounts to 3 ps. The much larger desorption time constant of the pentacarbonyl cluster can be explained by the larger number of degrees of freedom. Inelastic electron scattering processes with time constants below 130 fs precede the thermal desorption in both clusters. Using the measured dissociation rate constants and a statistical RRK analysis, a desorption energy of 0.91 eV for $Au_2(CO)^-$ and of 0.60 eV for $Pt_2(CO)_5^-$ has been derived. The low desorption threshold of $Pt_2(CO)_5^-$ suggests the loss of a terminal CO ligand. The metal-ligand desorption energies for $Pt_2(CO)_5^-$ and $Au_2(CO)^-$ are similar to the CO-desorption energies from the respective crystal surfaces.

We thank A. Bringer, Forschungszentrum Jülich GmbH (IFF), for stimulating and valuable discussions.

[1] G. Korzeniewski, E. Hood, and H. Metiu, J. Vac. Sci. Technol. **20**, 594 (1982).
[2] E. Knoesel, A. Hotzel, T. Hertel, M. Wolf, and G. Ertl, Surf. Sci. **368**, 76 (1996).
[3] M. Aeschlimann, M. Bauer, and S. Pawlik, Chem. Phys. **205**, 127 (1996).
[4] N. Pontius, P. S. Bechthold, M. Neeb, and W. Eberhardt, Phys. Rev. Lett. **84**, 1132 (2000).
[5] N. Pontius, G. Lüttgens, P. S. Bechthold, M. Neeb, and W. Eberhardt, J. Chem. Phys. **115**, 10 479 (2001).
[6] A. Grushow and K. M. Ervin, J. Chem. Phys. **106**, 9580 (1997).
[7] V. A. Spasov and K. M. Ervin, J. Chem. Phys. **109**, 5344 (1998).
[8] N. Pontius, P. S. Bechthold, M. Neeb, and W. Eberhardt, Appl. Phys. B **71**, 351 (2000).
[9] C. Y. Cha, G. Ganteför, and W. Eberhardt, Rev. Sci. Instrum. **63**, 5661 (1992).
[10] *Chemical Kinetics and Dynamics,* edited by J. I. Steinfeld, J. S. Francisco, and W. L. Hase (Prentice Hall, Upper Saddle River, NJ, 1998), Chap. 11.
[11] Vibrational energies of $Au_2(CO)^-$ using the GAUSSIAN98 program package: 1697 cm^{-1}, 385.6 cm^{-1} (Au-C), 257.6 cm^{-1}, 125.6 cm^{-1} (Au-Au), 67.6 cm^{-1}, 46.7 cm^{-1}.
[12] G. Lüttgens, N. Pontius, C. Friedrich, R. Klingeler, P. S. Bechthold, M. Neeb, and W. Eberhardt, J. Chem. Phys. **114**, 8414 (2001).
[13] H. Häkkinen and U. Landman, J. Am. Chem. Soc. **123**, 9704 (2001); and this work.
[14] J. J. Quinn, Phys. Rev. **126**, 1453 (1962).
[15] G. Schulze Icking-Konert, H. Handschuh, G. Ganteför, and W. Eberhardt, Phys. Rev. Lett. **76**, 1047 (1996).
[16] S. Roszak and K. Balasubramanian, J. Chem. Phys. **103**, 1043 (1995).
[17] Y. Y. Yeo, L. Vattuone, and D. A. King, J. Chem. Phys. **106**, 392 (1997).